Matter

CellPress

Article

Harnessing the wide-range strain sensitivity of bilayered PEDOT:PSS films for wearable health monitoring

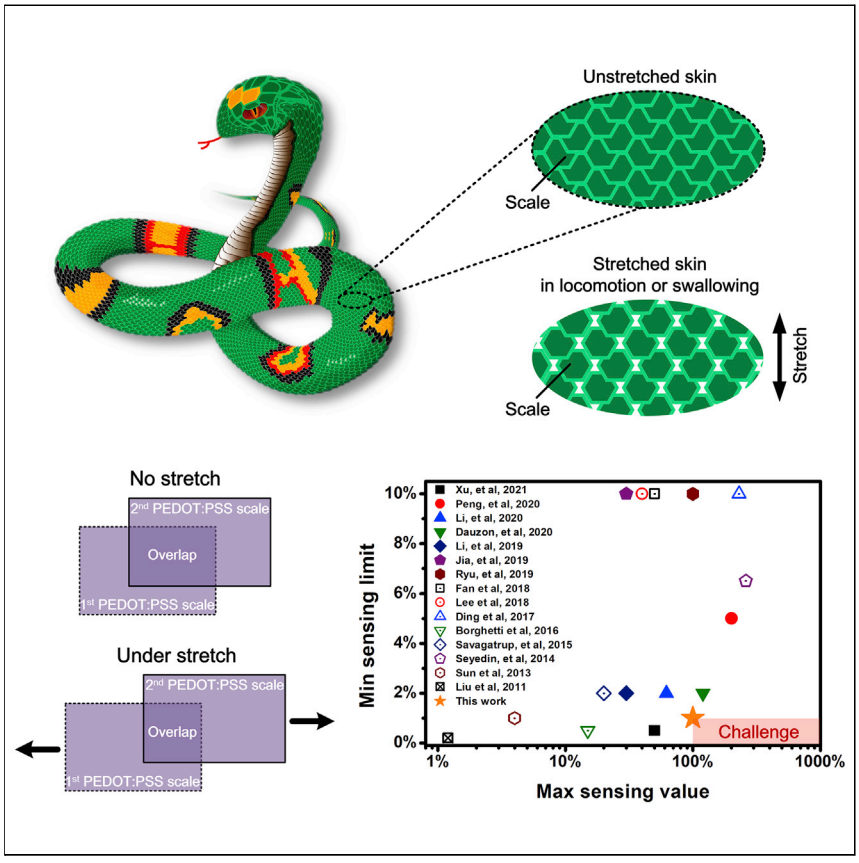

A bilayered PEDOT:PSS film that enables wide-range strain sensing is reported. With the dislocation of microcracked films under strain, low detection limit, and high maximum sensing value are realized simultaneously. The resultant wearable strain sensor is capable of perceiving phonation and facial expression.

Hao Liu, Shiming Zhang, Zhikang Li, ..., Mehmet Remzi Dokmeci, Feng Xu, Ali Khademhosseini

szhang@eee.hku.hk (S.Z.)
fengxu@mail.xjtu.edu.cn (F.X.)
khademh@terasaki.org (A.K.)

Highlights

A bilayered PEDOT:PSS film is engineered to enable wide-range strain sensing

A soft hydrogel layer is used to improve the device's coupling with skin

The sensor is capable of perceiving pulse patterns, phonation, and facial expression

Development
Practical, real world, technological considerations and constraints

Liu et al., Matter 4, 2886–2901
September 1, 2021
https://doi.org/10.1016/j.matt.2021.06.034

CellPress

Matter

Article

Harnessing the wide-range strain sensitivity of bilayered PEDOT:PSS films for wearable health monitoring

Hao Liu,[1,2,3,4,5] Shiming Zhang,[6,7,*] Zhikang Li,[3,4,5,12] Tian Jian Lu,[8] Haisong Lin,[9] Yangzhi Zhu,[7] Samad Ahadian,[3,4,5,7] Sam Emaminejad,[3,9] Mehmet Remzi Dokmeci,[4,5,7,10] Feng Xu,[1,2,*] and Ali Khademhosseini[3,4,5,7,10,11,13,*]

SUMMARY

Mechanical deformation of human skin provides essential information about human motions, muscle stretching, vocal fold vibration, and heart rates. Monitoring these activities requires the measurement of strains at different levels. Herein, we report a wearable wide-range strain sensor based on conducting polymer poly(3,4-ethylenedioxythiophene) polystyrene sulfonate (PEDOT:PSS). A bioinspired bilayer structure was constructed to enable wide-range strain sensing (1%–100%). Besides, hydrogel was chosen as the biological- and mechanical-compatible interface layer with the human skin. Finally, we demonstrated that the strain sensor is capable of monitoring various strain-related activities, including subtle skin deformation (pulse and phonation), mid-level body stretch (swallowing and facial expressions), and substantial joint movement (elbow bending).

Progress and potential

Wearable monitoring of skin deformations suggests insightful information about health status. However, realizing wide-range sensing with both low detection limit and high maximum sensing value has been challenging. In this work, bilayered microcracked PEDOT:PSS films are fabricated to mimic the scales of the snakeskin. The resultant sensors can detect wide-range strain with high resolution. Furthermore, a hydrogel layer is used to interface the device and skin for better biological and mechanical compatibility. Benefited from these merits, the sensors show excellent results in detecting various deformations of the skin for wearable health monitoring.

INTRODUCTION

Wearable devices have been attracting considerable interests during the past decade while finding extensive applications in personalized health monitoring, such as physiological sensing, neural modulation, and virtual/augmented reality.[1–5] The fabrication of wearable electronic devices favors soft and electrically conductive materials because of their amenable integration with the human skin. Among soft conductive materials, conducting polymers have a greater potential due to their mechanical flexibility, tunable conductivity, and solution processability.[6–11] In particular, poly(3,4-ethylenedioxythiophene) doped with polystyrene sulfonate (PEDOT:PSS) has higher conductivity and better stability in the conductive polymer family. It has been introduced as an ideal candidate for applications ranging from energy storage (e.g., supercapacitors[12–15] and solar cells[16–18]), electronic displays (e.g., light-emitting diodes[19–21] and electrochromic devices[22–24]), to organic electrochemical transistors.[25–29] In recent years, to meet the increasing demand for personalized health monitoring, PEDOT:PSS has also been utilized in wearable strain sensors to monitor gestures or tactile pressure.[30–32]

Strain levels of different parts of the human body indicate a variety of physical or physiological indexes closely correlated with health status.[33–35] For example, measuring strains at joints of fingers and limbs offers insightful information for evaluating the performance of athletes and the rehabilitation efficacy of patients. The levels of epidermal strain at the wrist are relevant for heart rate monitoring and cardiovascular function assessment. Similarly, subtle strains of facial expressions may

provide clues to reveal hidden emotional fluctuations.[36–39] It is noteworthy that strain levels vary significantly between different sites of the human body. For example, when conducting daily activities, the strain applied onto limb joints can be up to 100%, while the strain induced by heartbeat-triggered subcutaneous artery expansion onto the skin of the wrist is usually less than a few percent.[40,41] Therefore, there is a growing desire to engineer wearable wide-range strain sensors that can match the diverse sensing needs at different locations of the human body.

Aiming toward strain-sensing devices with wide detection ranges, several PEDOT:PSS-based strain sensors have been developed for wearable applications. For instance, ultra-sensitive devices with a low limit of detection of less than 1% (e.g., down to 0.2% strain) have been fabricated to sense minute human movements.[42–44] However, due to the intrinsically poor stretchability of PEDOT:PSS, these sensors are prone to deterioration in performance or even experience functional failure under relatively large levels of strain (>20%).[45] To improve the stretchability of the device, PEDOT:PSS has been dispersed in highly stretchable elastomer networks (e.g., polyurathene) to prepare conductive composite fibers. By homogenously dispersing conductive fillers in the elastomer, the composite fiber showed excellent electrical (~25 S cm^{-1}) and mechanical properties, which enabled it to work under substantial strains up to 260%.[46,47] However, the ability to detect lower strain values turned out to be compromised (unable to measure strains <10%), impeding its application in accurate strain sensing of subtle activities (like pulse and phonation). Therefore, it remains an unsolved challenge to achieve wide-range strain sensing with PEDOT:PSS.

The skin of some reptiles (such as snakes) is covered with imbricate scales that can move away from each other to accommodate the tension of the skin, which contributes to an improved stretchability (Figure 1A).[48,49] Inspired by this unique structure, we herein propose a bilayered PEDOT:PSS film for strain sensing. In this construct, micro-size PEDOT:PSS islands are percolatively connected to confer a high stretchability of the bilayered film. The density of these micro-islands affects the stretchability of the film, which could be modulated by the combination of pre-stretching and multi-step spin-coating processes. The relative displacement of overlapping PEDOT:PSS micro-islands can be induced by small strains, while the proposed strain sensor can also handle large strains with structural and functional robustness. This mechanism enabled the PEDOT:PSS-based strain sensor to perform reliably over a wide range of strains. In the meantime, the sensitivity and stability of the sensor were evaluated. A hydrogel layer was introduced below the device as an interface layer between the sensing element and the human skin to improve the biological and mechanical compatibility of this strain sensor. Tensile and lap shear tests were conducted to investigate the robustness and reliability of the elastomer/hydrogel interface. Finally, the sensor was deployed on the human body to evaluate its ability in sensing various skin deformations.

RESULTS AND DISCUSSION

Fabrication of the bilayered PEDOT:PSS strain sensor

As demonstrated in Figure 1B, the fabrication process of the PEDOT:PSS strain sensor started by treating the surface of the elastomer substrate (polydimethylsiloxane [PDMS] or VHB tape) with O_2 plasma to improve its hydrophilicity and to allow PEDOT:PSS to better attach to the elastomer surface. Next, a layer of PEDOT:PSS was spin coated onto the treated elastomer, baked, and uniaxially stretched (50% strain) to produce fractures. As a result, areas between neighboring PEDOT:PSS islands on

[1]The Key Laboratory of Biomedical Information Engineering of Ministry of Education, School of Life Science and Technology, Xi'an Jiaotong University, Xi'an 710049, P.R. China

[2]Bioinspired Engineering and Biomechanics Center (BEBC), Xi'an Jiaotong University, Xi'an 710049, P.R. China

[3]Department of Bioengineering, University of California-Los Angeles, Los Angeles, CA 90095, USA

[4]Center for Minimally Invasive Therapeutics (C-MIT), University of California-Los Angeles, Los Angeles, CA 90095, USA

[5]California NanoSystems Institute, University of California-Los Angeles, Los Angeles, CA 90095, USA

[6]Department of Electronic and Electrical Engineering, The University of Hong Kong, Hong Kong SAR, P.R. China

[7]Terasaki Institute for Biomedical Innovation, 11570 W Olympic Boulevard, Los Angeles, CA 90024, USA

[8]State Key Laboratory of Mechanics and Control of Mechanical Structures, Nanjing University of Aeronautics and Astronautics, Nanjing 210016, P.R. China

[9]Department of Electrical and Computer Engineering, University of California-Los Angeles, Los Angeles, CA 90095, USA

[10]Department of Radiology, University of California-Los Angeles, Los Angeles, CA 90095, USA

[11]Department of Chemical and Biomolecular Engineering, University of California-Los Angeles, Los Angeles, CA 90095, USA

[12]School of Mechanical Engineering, Xi'an Jiaotong University, Xi'an, 710049, China

[13]Lead contact

*Correspondence: szhang@eee.hku.hk (S.Z.), fengxu@mail.xjtu.edu.cn (F.X.), khademh@terasaki.org (A.K.)

https://doi.org/10.1016/j.matt.2021.06.034

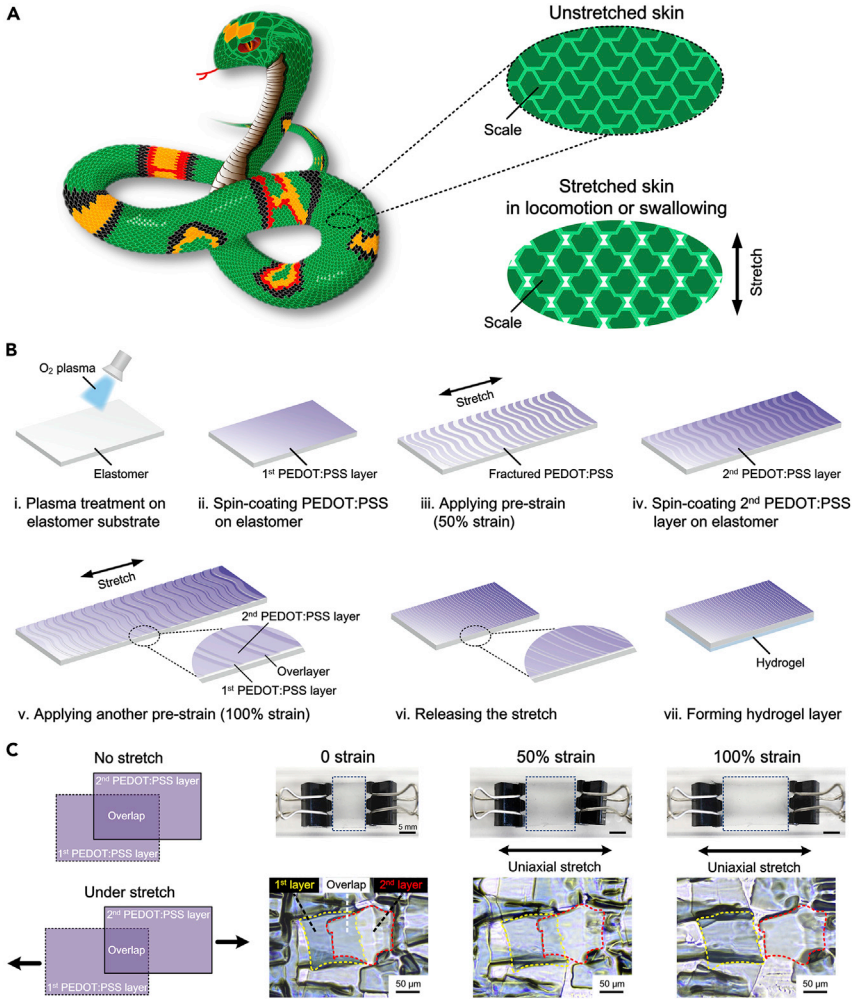

Figure 1. The mechanism of wide-range strain sensing with PEDOT:PSS

(A) Schematic of the imbricate scaly skin of a snake. The enlarged schemes show the relative displacement of overlapped scales when the skin is under strain.

(B) Schematic demonstration of the fabrication process of the wide-range PEDOT:PSS strain sensor with bilayer, overlapping structure.

(C) Scheme, digital photos, and optical microscopy images of the strain sensor under strain. The dotted lines clearly outline the two overlapped PEDOT:PSS islands (yellow, from the first layer; and red, from the second layer) that move away from each other under stretch, resembling the relative displacement of scales on snake skin.

the elastomer were exposed to provide bonding sites for the following deposition of a second PEDOT:PSS layer. After spin coating of the second PEDOT:PSS layer, the PEDOT:PSS/elastomer was baked and further stretched (100% strain). During this procedure, the second PEDOT:PSS layer cracked into islands, which created overlapping areas with those from the first layer. Subsequently, the pre-stretch was released, and a bilayer, scaly structure with overlapping microscale PEDOT:PSS islands was produced (Figure S1). Additional proof-of-concept demonstrations showed that the top PEDOT:PSS layer can be readily peeled off from the bottom one, and validated that the two-step spin coating of PEDOT:PSS resulted in a bilayer construct capable of interlayer movement, rather than a monolayer, merged PEDOT:PSS film (Figure S2; Movie S1). In this bilayer structure, not only islands from different PEDOT:PSS layers overlapped with each other, but those of the second layer also self-aligned due to the pre-stretch effect.

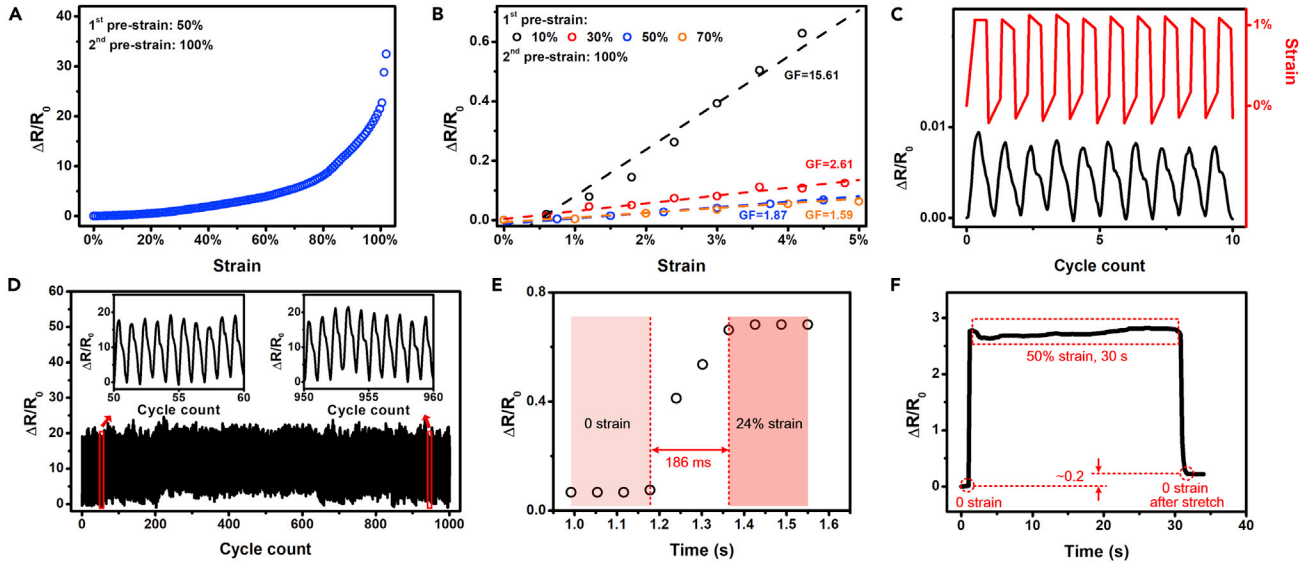

Figure 2. Electrical performance of the PEDOT:PSS-based strain sensor

(A) Relative resistance changes of the sensor versus different strain levels (first pre-strain, 50%; second pre-strain, 100%).

(B) Sensitivities of the sensor in strain ranges under 5%. Gauge factors are given by the slope of the linearly fitted results. The first pre-strain levels ranged from 10% to 70%, and the second pre-strain level was fixed at 100%.

(C) Relative resistance change of the sensor to small strains (down to 1%).

(D) Cyclic performance of the sensor under 100% strain for 1,000 cycles of stretch/release.

(E) Characterization of the response time of the sensor facing 24% strain.

(F) Strain-sensing performance of the sensor under long-term strained state (at 50% strain for 30 s).

For data shown in (C–F), the first pre-strain was 50% and the second pre-strain was 100%.

Finally, a biocompatible hydrogel layer was spin coated and cured at the bottom of the elastomer, which concluded the fabrication of the biocompatible PEDOT:PSS/elastomer/hydrogel multilayered strain sensor.

Working mechanism and sensing performance of the strain sensor

The working principle of the proposed strain sensor was based on the displacement of overlapping PEDOT:PSS islands under mechanical stretch. Specifically, stretching the sensor resulted in the slipping of adjacent overlapping islands, which decreased the overlayer area (Figure 1C). Accordingly, the contact resistance between the overlapping areas increased, and it was reflected by the change of the total resistance of the device. Since the maximum sensing range of the sensor was determined by the initial (0 strain) overlapping area of PEDOT:PSS layers, which was related to the strain level of the first pre-stretch, it was essential to investigate the sensor performance under different pre-strain levels (Figures 2A and S3). As shown in the results, pre-strains of 50% and 70% promised the maximum sensing value to be over 100% strain. While, on the other hand, sensors fabricated with smaller pre-strains (i.e., 30% and 10%) failed to work when strain levels merely exceeded a low value (i.e., ~39% and ~13%), due to the entire disconnection of neighboring PEDOT:PSS islands within the conductive structure. Despite its inferiority in sensing large strains, the 10% pre-strain sensor exhibited a remarkably improved sensitivity (gauge factor of 15.61) in detecting small strains (<5%) compared with its counterparts, i.e., gauge factors of 2.61, 1.87, and 1.59 for the 30%, 50%, and 70% pre-strain groups, respectively (Figure 2B). Such an intriguing phenomenon is associated with the morphology effect where lower pre-strain levels lead to a smaller overlap between adjacent PEDOT:PSS islands and thus ease the separation of the overlapping

islands under stretch. And the resistance rises drastically after the morphological separation at the microscale, because of less conducting routes for charge carrier transfer inside PEDOT:PSS. Such flexible tunability in sensitivity at small strains coupled with maximum sensing range provided an exciting opportunity in selecting sensors for different applications.

To systematically investigate the sensing performance of the PEDOT:PSS strain sensor in depth, we analyzed responses of the sensor at different strain ranges. Intriguingly, the sensing curve can be divided into two different phases under mechanical loading. In specific terms, the relative resistance changes of the sensor increased linearly during small strains, while a sharp and exponential rise in resistance was observed when the strain level surpassed a threshold (Figure S4). An example is that, for the sensor made with first pre-strain of 50%, a linear resistance increase with gauge factor of 2.91 (R^2 = 0.9709) can be observed for strains lower than 24% and, once over this critical strain, the sensing data can be found to match with the exponential fitting curve (R^2 = 0.9798). Such a unique feature was attributed to the bilayered PEDOT:PSS sensing structure where conductive micro-islands overlap. Under small strains, electrical currents can travel through the overlapped PEDOT:PSS islands (Figure S5), and the total resistance is dominated by the contact resistance of the overlapping regions, which was proved to be ~30 times greater than the resistance of a single PEDOT:PSS island (Figure S6). Since the contact resistance is proportional to the applied strain levels,[50] the total resistance presented a linear increase along with strains. However, when experiencing larger strains, overlaps in the PEDOT:PSS bilayer structure decreased and disconnections of neighboring islands began to appear (Figure 1C), weakening the influence of contact resistance on the total value. On the other hand, cracks formed and propagated on PEDOT:PSS, making the conduction route on the PEDOT:PSS island tortuous, resembling a sine curve (Figures S5 and S7). In this way, the relative resistance change, as a function of applied strain, increased exponentially[51] and agreed well with the exponential fitting data when the strain level exceeded a critical value; and, according to the data displayed in Figure S4, this threshold can be adjusted by tuning the strain level of first pre-stretch, with threshold values of 4%, 15%, 24%, and 47%, corresponding to first pre-strains of 10%, 30%, 50%, and 70%, respectively. It is also worth noting that, under intense stretch (e.g., 100% strain), more overlapping PEDOT:PSS islands separated from each other (Figure 1C), causing remarkably weakened electrical connection and thus significantly increased resistance (Figure 2A).

As for the effect of the second pre-strain level on sensing performance, since larger pre-strains lead to an increased number of islands with smaller sizes generated during the fabrication process, improving the density of PEDOT:PSS micro-islands in the conductive network, larger pre-strains yield higher maximum sensing limit and wider range of the sensor (Figure S8). But, considering the viscoelastic behavior of the elastomer substrate whose detrimental effect to the long-term performance of the sensor is aggravated at large strains, a moderate second pre-strain level (i.e., 100%) that can meet the demand of wide sensing range (i.e., 1%–100% strain) is appreciated. Apart from pre-strain levels, experimental parameters, such as plasma treatment time and spin-coating speed, were also optimized (Figures S9–S12). Detailed explanations can be found in the supplemental information.

Meanwhile, the ability to detect small deformations (<5% strain) was demonstrated by its high and tunable sensitivity (i.e., gauge factors of 1.59–15.61) in small strain sensing (Figure 2B) and reliable performance (relative resistance change of ~1%)

responding to small strains down to 1% (Figure 2C). In this way, the need of sensing ultralow-level strains on human skin can be fulfilled to benefit healthcare assessment of physiological conditions and emotional states. The conventional PEDOT:PSS strain sensors reported in previous works were associated with deficiencies in realizing wide-range sensing,[42–47,52–60] which were only available in limited working regions that are either too small (0.2%–20% strain) or too large (10%–260% strain). Compared with these counterparts, the developed device with a snake-skin-inspired sensing structure presented a wide-range sensing performance that combined a low minimum detection limit (1% strain) and a high maximum sensing value (100% strain) (Figure S13). This is a significant improvement in sensing range (1%–100% strain) for PEDOT:PSS-based strain sensors, which provides a promising approach for full-range sensing of human skin strains. In the meantime, employing the bilayer PEDOT:PSS structure was shown to be advantageous in sensing over a wide range of strain levels as compared with directly spin coating a single layer of PEDOT:PSS on an elastomer substrate (Figure S14). The cyclic performance is a key parameter to evaluate the long-term robustness of strain sensors and allows for propelling cutting-edge research prototypes toward practical applications. As shown in Figure 2D, the sensor could tolerate as many as 1,000 repeated cycles of strains as large as 100%, with negligible performance loss. This exceptional functional stability over cyclic mechanical loading/unloading supports the use of the proposed sensors for extended practical applications.

In addition, the sensor showed a quick response to strains with a response time of ~186 ms (Figure 2E), making it suitable for high-frequency monitoring. To investigate its performance under a long-term strained state, the sensor was first stretched to 50% strain, holding for 30 s, and then released. A slight drift of the signal (~0.2) can be observed after releasing the strain, compared with the initial state before stretch (Figure 2F). Such a rise in resistance can be explained by the decrease of overlapping area after the long-term strained state compared with the original unloaded state (Figure S15), resulting from viscoelasticity of PDMS and the strong adhesion between PEDOT:PSS and PDMS. Although such a signal drift is unexpected, especially for cases where large strains and longer periods are required, its impact on wearable applications should be alleviated since the human body is continuously moving and it is not common to see a specific, large strain for a long time in daily activities. On the other hand, for those application cases requiring ultra-high sensitivity and reliability, this sensor can be used in a disposable way, benefiting from its low cost and easy fabrication features. Also, as a result of the synergy of the viscoelastic property of PDMS and strong bonding of the PDMS/PEDOT:PSS interface, the PEDOT:PSS islands cannot rapidly move back to their initial positions upon releasing the strain on the sensor,[61] and hysteresis can be thus induced (Figure S16).

Mechanical characterization of the elastomer/hydrogel interface of the strain sensor

To build a human-friendly interface for wearable applications, a hydrogel layer was integrated to the bottom of the sensor. Indeed, the inherently biocompatible feature and skin-like mechanical property of hydrogels promote conformal human-sensor integration and a comfortable user experience.[36,62] A commonly used method for polymer grafting via benzophenone (BP) treatment was adopted to realize elastomer-hydrogel bonding.[63–65] Since the hydrogel layer was integrated onto the elastomer layer of the sensor, it was necessary to investigate the mechanical properties (i.e., tensile performance and adhesion strength) of the elastomer/hydrogel hybrid. Various elastomers, such as PDMS and VHB tape, and hydrogels,

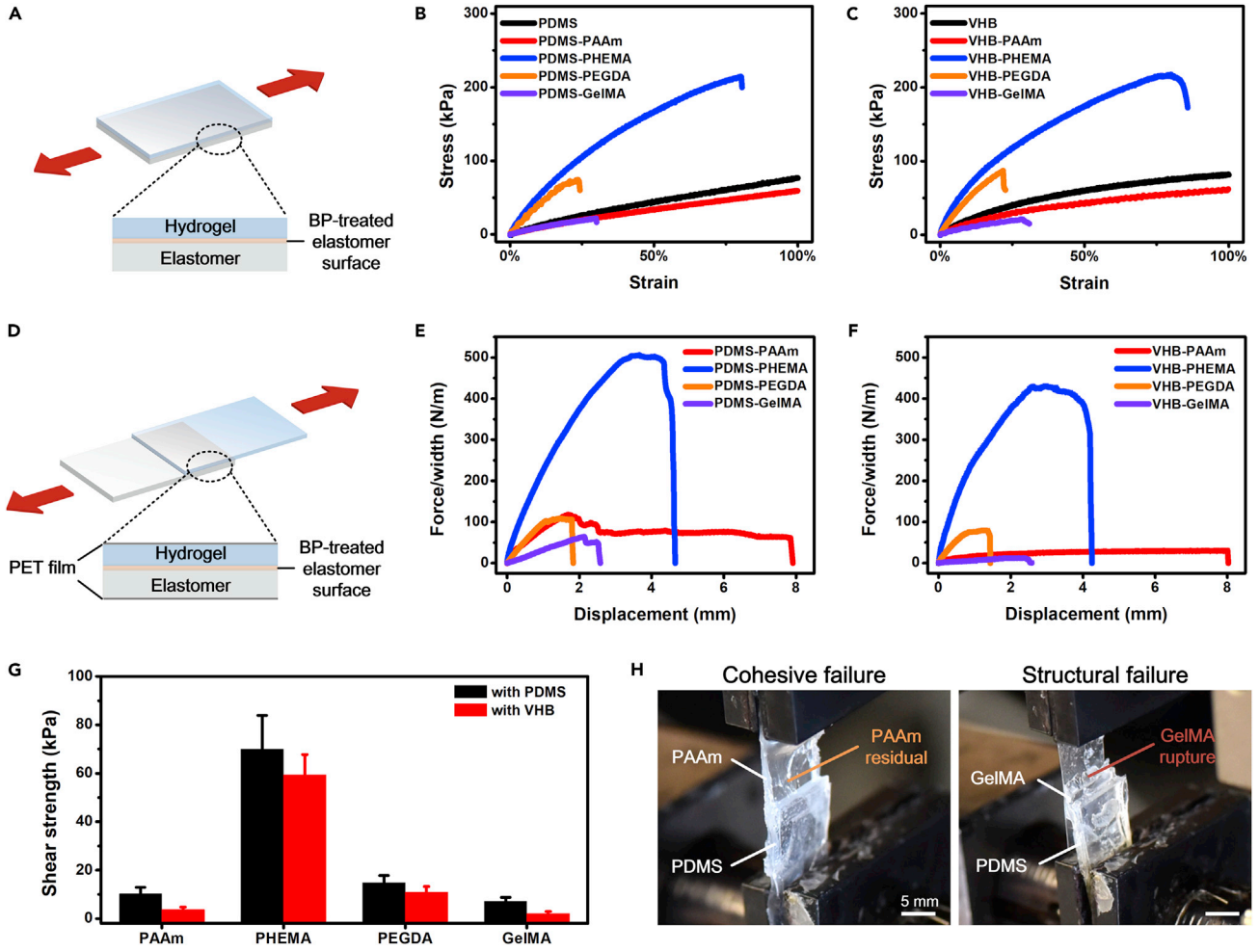

Figure 3. Mechanical characterization of the elastomer/hydrogel hybrid of the PEDOT:PSS-based strain sensor

(A–C) Tensile test of the elastomer/hydrogel hybrid: schematic diagram (A) and experimental data of PDMS/hydrogel (B) and VHB/hydrogel (C) hybrids.

(D–F) Lap shear test of the elastomer/hydrogel hybrid: schematic diagram (D) and experimental data of PDMS/hydrogel (E) and VHB/hydrogel (F) hybrids.

(G) Shear strength of different elastomer/hydrogel hybrids obtained from the lap shear test results. Error bars represent standard deviation ($N = 5$).

(H) Digital photos of different failure modes of elastomer/hydrogel hybrids. Left: cohesive failure of PDMS/PAAm. Right: structural failure of PDMS/GelMA.

including polyacrylamide (PAAm), polyhydroxyethyl methacrylate (PHEMA), polyethylene glycol diacrylate (PEGDA), and gelatin methacryloyl (GelMA), could be used for creating mechanically robust elastomer/hydrogel interfaces. As depicted in Figure 3A, the BP-bonded elastomer/hydrogel bilayer was uniaxially stretched during the tensile test. Because both PDMS and VHB are ultra-stretchable and can tolerate strain levels of more than 100%, the stretchability of the bilayer was largely dependent on the maximum strain that the hydrogel could sustain before it fractured. Among all the elastomer/hydrogel groups, elastomers bonded with PAAm were optimal for wide-range strain sensing since these can endure strains with a higher limit of up to 100% (Figures 3B and 3C). Although PHEMA showed comparable stretchable characteristics (~80% strain) when integrated with elastomers, its Young's modulus (~600 kPa) was too high to interface with the human skin (<100 kPa) (Figure S17). This mismatch in modulus also set a hurdle for PEGDA to be used for on-skin applications. GelMA is soft enough, despite its inferior

stretchability (breaks at less than 30% strain), making it a potential candidate for small strain detection.

To characterize the adhesion strength of the elastomer/hydrogel attachment, a lap shear test was carried out to mimic the shear deformation that would be experienced during practical on-skin applications (Figure 3D). To prevent the elongation of the hydrogel and the elastomer during shear peeling, which is expected to produce errors in measuring the adhesion strength, the top surface of the hydrogel and the bottom surface of the elastomer were both glued with a thin PET film. According to the test results, the bonds between PAAm and elastomers had the highest endurance to shear peeling, which failed after ~8 mm of displacement (length of the overlap, 7 mm) (Figures 3E and 3F). Although elastomers bonded with PHEMA demonstrated remarkably higher shear strengths (~70 kPa) compared with elastomers bonded with other hydrogels (<20 kPa) (Figure 3G), the maximum shear displacement at which the two layers totally detached was less than 5 mm. When the elastomer was bonded with PEGDA or GelMA, the shear adhesion performance failed within 3 mm. Such a significant difference can be explained by the different failure modes of hydrogel-elastomer adhesion during peeling (Figure 3H). When peeled from the PDMS elastomer, the PAAm hydrogel experienced cohesive failure, leaving hydrogel residues on the elastomer surface. This helped the hydrogel to sustain a larger amount of peeling force, which was probably coming from the dissipative network of PAAm. While, for other hydrogels, different mechanisms for hydrogel/elastomer adhesion failure existed. Taking GelMA as an example, it ruptured when the peeling force exceeded its mechanical strength, and thus suffered a structural failure.

Functional demonstration of the strain sensor for wearable health monitoring

To demonstrate its applications in wearable healthcare monitoring, two copper wires were integrated at the PEDOT:PSS sensing bilayer and two additional PDMS islands were further coated on top of the device (at both ends) for encapsulation (Figure 4A). The copper wires connected the device with external circuitry and transmitted strain-induced resistance changes to detect the strain. During wearable uses, the sensor was directly attached to the human body where the bottom hydrogel layer (i.e., PAAm) interfaced with skin (through van der Waals force) in a conformal and comfortable manner. To demonstrate the feasibility of wide-range strain sensing in practical wearable health monitoring, multiple human activities with varying degrees of strain, including pulse and phonation with small strains, swallowing and facial expression with mid-level strains, and limb movement with substantial strains, were detected with the proposed sensor to uncover insight on physical and psychological well-beings (Figure 4B). Pulse rate is a well-known and easily accessible parameter to monitor cardiovascular health, and it can be utilized to identify problems, such as dizziness, internal bleeding, and high blood pressure. As shown in Figure 4C, the sensor attached at the wrist could detect pulse rates under different conditions (i.e., at rest and right after a workout). According to the data, the different physical states of the human body can be readily distinguished in terms of frequency and amplitude. More specifically, the pulse rate at rest was ~60 bpm, while the data after a workout (30 push-ups) increased to ~80 bpm. In addition, it can be obtained from the standard sensing curve that the strain induced by pulse rose from ~1% (at rest) to ~10% (after workout). Such a phenomenon can be explained by the increased level of oxygen consumption and further enhanced blood pumping triggered by physical exercises. Note that the two pulse wave peaks, namely P1 and P2, can be easily identified by an untrained eye and can be used to provide detailed information about cardiovascular health with further analysis.[66]

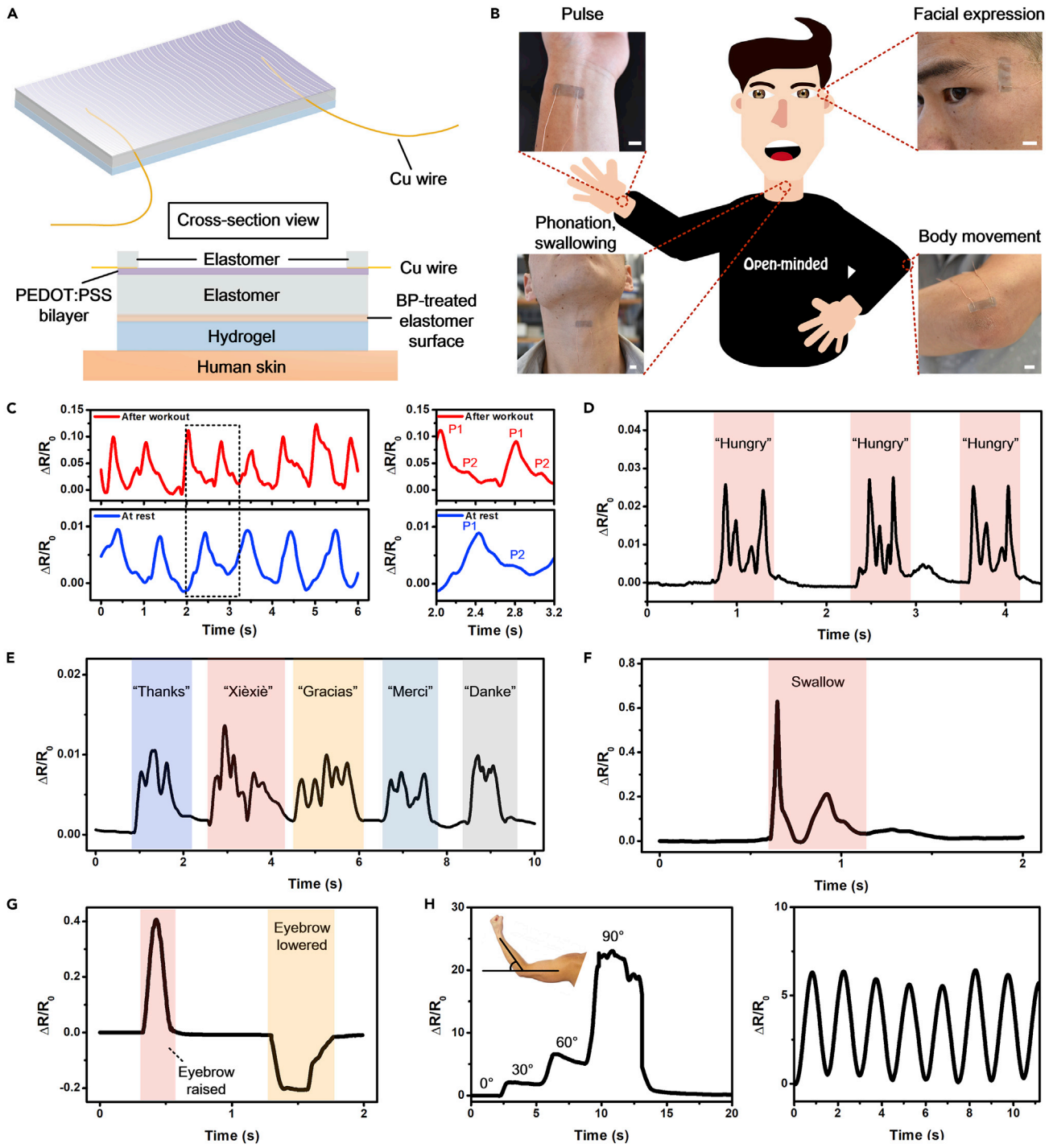

Figure 4. Wearable applications of the PEDOT:PSS-based strain sensor

(A) Schematic of the sensor structure for wearable strain sensing.

(B) Schematic and digital photos of sensors attached to different parts of human body for sensing of various signals. Scale bar, 1 cm.

(C) Pulse signal under different physical conditions (at rest and after doing 30 push-ups). Right: enlarged view of the sensing data indicated by the dotted rectangle in the left plot.

(D) Phonation sensing data when reading the same word for three times.

(E) Phonation sensing data when reading different words.

Figure 4. *Continued*
(F) Swallowing monitoring realized by adhering the sensor at the throat.
(G) Sensing data of facial expressions resulting from stretch and compression of skin by raising or lowering the eyebrow, respectively.
(H) Limb movement detected with the PEDOT:PSS-based strain sensor. The inset schematic describes the bending angle of the elbow. Right: response of the sensor to bending the elbow to 60° seven times.

For people unable to speak as a result of larynx injury or laryngectomy, a hand-held device is usually needed to help produce speeches through placing it against the neck to vibrate and make sounds when moving the tongue and mouth. Regardless of the portability of this miniaturized device, training from a professional speech therapist and significant practice are required. To solve this problem, emerging wearable sensors that can detect low levels of tissue deformation during phonation and function in an imperceptible manner may present as a promising solution. To investigate the potential of the proposed strain sensor for phonation sensing, the sensor was placed at the vocal cord. And we recorded resistance changes while reading the word "hungry" three times. Experimental results in Figure 4D indicated that the sensor showed decent repeatability with highly similar signals detected for each reading. Furthermore, since reading "thanks" in different languages, including English ("thanks"), Chinese ("xièxiè"), Spanish ("gracias"), French ("merci"), and German ("danke"), can result in the deformations of the skin covering the vibrating vocal cord, the corresponding strain-induced signal changes may shed light on the different vocalization patterns (Figure 4E). Such a satisfactory performance unveils the potential of the as-fabricated sensor for voice recognition and auxiliary phonation purposes. It is also anticipated to aid effective communications for those working in noisy conditions, such as firefighters, ground staff in airports, and security services in shopping malls, by acquiring speeches directly from the speaker without signal loss during airborne transmission.

In addition to the ability to detect very small strains (<10%) of the human body, the sensor can also detect mid-range (10%–40%) and large (>40%) strains. During swallowing, the skin on the throat experienced a tensile strain of about 10%–30%, which resulted in a relative resistance change from 0.2 to 0.65, according to the data picked up by the sensor (Figure 4F). It is noteworthy that the two signal peaks appearing in the plot were associated with the upward and then the downward movement of the larynx in the pharyngeal phase of swallowing, respectively. To monitor facial expressions, the sensor was attached to the skin near the temple, as demonstrated in Figure 4A. When the eyebrow was raised, the sensor was stretched to conform to the deformations of the skin, which directly led to an increase in the sensor's resistance (Figure 4G). While the lowered eyebrow, corresponding to actions, such as frowning, resulted in the compression of the skin-attached sensor and thus yielded a decrease in resistance. Interestingly, raising and lowering eyebrows can be utilized to articulate emotions of excitement and suffering, respectively. Therefore, this finding is promising to widen the application space of wearable sensors, from currently available external physical and physiological monitoring to discovering internal emotions and related psychological cues. To demonstrate the ability to detect large strains, elbow bending was monitored. The measurements indicate that the proposed sensor was reliable to differentiate between various bending angles. Specifically, relative resistance changes of 1.92, 6.42, and 22.21, respectively, corresponded to bending angles of 30°, 60°, and 90°, which induced strain levels of 45%, 74%, and 100% (Figure 4H). In addition, the cyclic stability of the sensor during mechanical loading was evaluated. We did not observe any significant degradation in device performance, which takes this sensor a step closer as a wearable device for motion detection.

Overall, the key contribution of this work is proposing a general strategy to realize a wide working range for strain sensors through combining sensitive detection at small strains and stable performance at large strains, based on a bioinspired, bilayered, and overlapping PEDOT:PSS structure. Realizing low detection limit and high maximum sensing value simultaneously to yield wide-range sensing was a critical challenge for developing versatile strain sensors. This conundrum is especially intractable for those aiming at wearable applications where a wide range of strain levels on different parts of the human body are required to be recorded. Mimicking the natural dermal armor of reptiles (such as snakes), which aids locomotion and ingestion by the relative movement of overlapping scales on the skin, we have successfully fabricated a bilayered, overlapping PEDOT:PSS structure that has shown promising results to measure a wide range of strains with high resolution.

Another significant point that deserves emphasis is deploying a biocompatible hydrogel layer as an interface between the sensing device and the human skin. In this work, a series of hydrogels (i.e., PAAm, PHEMA, PEGDA, and GelMA) were tested as intermediate layers to establish a human-machine interface, and the differences in their mechanical properties provided flexibility in materials selection to meet different demands of specific applications. As the interface to transfer strain from skin to the device, hydrogels with small thickness and low modulus are appreciated to yield a better strain transfer effect and thus improved sensing performance (Figure S18). Further employment of an adhesive hydrogel contributed to robust bonding between sensor and human skin, and the adhesion strength can be well maintained without significant decline despite skin perspiration, which is commonly known to weaken the interfacial adhesion due to the occurrence of water (Figures S19 and S20). Such an exciting finding offers promising opportunities for the proposed sensor to practical wearable uses. Although the dehydration of hydrogel in ambient conditions may stiffen the gel and affect the durability of the sensor, the emerging organohydrogel with a dual-solvent system of mixed water and organic solvents, such as glycerol, may present a way out. The introduced glycerol would bond with water molecules via hydrogen bonding and mitigate water evaporation from the polymeric network to yield a well-maintained mechanical softness (Figure S21), making it promising for fabricating sensors that would serve in long-term monitoring applications.

In addition, the fabrication process of the sensor is of low cost and easy accessibility because PEDOT:PSS is solution-processable and the sensor can be readily obtained via spin coating and baking. The optical transparency of components in the sensor system (including PEDOT:PSS, PDMS, and hydrogel) also aids some imperceptible and invisible applications of transparent bioelectronics.

Conclusion

In this work, we have presented a facile tactic to fabricate wearable, wide-range strain sensors with PEDOT:PSS. Circumventing the inherently poor stretchability of PEDOT:PSS, a bilayered, overlapping conducting layout that mimics the imbricate scaly skin of snakes was proposed to realize a low minimum detection limit (1% strain) and a high maximum sensing value (100% strain) at the same time. Meanwhile, the sensing performance of the device over such a wide strain range demonstrates adjustable sensitivity (gauge factor of 1.59–15.61) and functional stability (up to 1,000 times of cyclic stretch). To further propel the as-designed sensor to wearable applications, a hydrogel layer was integrated into the device, serving as a human-friendly intermediate layer to bridge the electronic device to the human body. The stretchable feature and robust adhesion of the sensor/hydrogel hybrid allow the device to operate under

different sensing ranges experienced by the human body. The high sensitivity over a wide spectrum of strain levels presents an attractive feature for wearable healthcare applications, as this smart gadget alone can provide insightful information about the physical status and psychological conditions of the user.

EXPERIMENTAL PROCEDURES

Resource availability

Lead contact

Further information and requests for resources and reagents should be directed to and will be fulfilled by the lead contact, Ali Khademhosseini (khademh@terasaki.org).

Materials availability

PDMS (Sylgard 184) was purchased from Dow Corning. VHB tapes were purchased from 3M. PEDOT:PSS (Clevios PH1000) was purchased from Heraeus. Glycerol, acrylamide, *N*,*N*′-methylenebisacrylamide, ammonium persulfate, *N*,*N*,*N*′,*N*′-tetramethylethylenediamine, hydroxyethyl methacrylate, ethylene glycol dimethacrylate, ethylene glycol diacrylate, GelMA, and Irgacure 2959 were purchased from Sigma-Aldrich. Benzophenone was purchased from Tokyo Chemical Industry. Cyanoacrylate adhesive (Loctite 406) was purchased from Henkel.

Data and code availability

The data that support the plots of this study may be reasonably requested from the corresponding authors.

Fabrication of the wide-range PEDOT:PSS strain sensor

Two materials, PDMS and VHB, were selected as candidates for elastomer in this study. VHB can be used as is, while a two-step fabrication process, spin coating (1,000 rpm, 30 s) and curing (80°C, 1 h), is needed to obtain a PDMS film before further treatments. The mass ratio of PDMS base to curing agent is 20:1. The size of the elastomer used here is 24 mm in length and 14 mm in width. To start, an oxygen plasma treatment (gas at 10 cc/min for 2 min, PE-25, Plasma Etch) was carried out for elastomer surface modification. Next, PEDOT:PSS mixed with glycerol (5%, v/v) and capstone (1%, v/v) was spin coated (3,000 rpm, 30 s) on the treated elastomer and then baked (130°C, 10 min). In the following step, the PEDOT:PSS-coated elastomer was stretched (10%, 30%, 50%, and 70% strain) and fixed at the pre-strain level by clamps to experience an additional PEDOT:PSS deposition (spin coating at 3,000 rpm for 30 s and then baking at 80°C for 1 h). Subsequently, the as-fabricated hybrid with the PEDOT:PSS bilayer on an elastomer substrate was further stretched to 100% strain. After releasing the strain, the bilayer conducting layout with overlapped PEDOT:PSS micro-islands was realized. Then two copper wires were integrated through coating and curing of a PDMS encapsulation island at both ends of the top surface of the hybrid.

To enhance the biocompatibility of the interface with human skin, a hydrogel layer was bonded to the bottom of the strain sensor. Hydrogels used in this work include PAAm, PHEMA, PEGDA, and GelMA. Before hydrogel bonding, the bottom surface of the elastomer was treated with oxygen plasma and benzophenone (BP, 10 wt % in ethanol). Next, a hydrogel precursor solution was spin coated (1,000 rpm, 30 s) on the BP-treated elastomer surface, and cured under UV exposure (365 nm, S2000, OmniCure) to achieve bonding. The precursor solutions of different hydrogels were prepared as follows: PAAm (20 wt % AAm, 0.03 wt % *N*,*N*′-methylenebisacrylamide as crosslinker, 0.1 wt % ammonium persulfate as thermal initiator,

and 0.1%, v/v, *N*,*N*,*N*′,*N*′-tetramethylethylenediamine as accelerator), PHEMA (60%, v/v, HEMA, 0.06%, v/v, ethylene glycol dimethacrylate as crosslinker, and 0.2 wt % Irgacure 2959 as photoinitiator), PEGDA (20%, v/v, PEGDA 700 and 0.2 wt % Irgacure 2959 as photoinitiator) and GelMA (10 wt % GelMA and 0.2 wt % Irgacure 2959 as photoinitiator). All experiments were carried out under ambient environmental conditions (25°C and ~50% relative humidity) without further declarations.

Tensile test of the elastomer/hydrogel hybrid

Tensile tests of the elastomer/hydrogel hybrid of strain sensors were conducted with a universal mechanical testing system (INSTRON 5943). As demonstrated in Figure 3A, samples for tensile tests were uniformly molded in a rectangular shape (length, 18 mm; width, 9 mm; and thickness, 2 mm: 1 mm thick elastomer and 1 mm thick hydrogel). Each sample was fixed to clamps of the tensile instrument and uniaxially stretched at a constant velocity (10 mm min^{-1}). The stress–strain data were recorded while performing the mechanical tensile test. Then the Young's modulus value was determined as the average slope over the 0%–10% strain range of the stress–strain curve.

Lap shear test of the elastomer/hydrogel hybrid

Lap shear tests of the elastomer/hydrogel hybrid of strain sensors were conducted with a universal mechanical testing system (INSTRON 5943). As demonstrated in Figure 3D, samples for lap shear tests were uniformly molded in an overlapped rectangular shape (total length of 29 mm: 18 mm long elastomer and hydrogel with 7 mm long overlapped area, width of 9 mm and thickness of 2 mm: 1 mm thick elastomer and 1 mm thick hydrogel). As stiff backings, thin PET films were glued to both the top and bottom surfaces of the elastomer/hydrogel bilayer hybrid by cyanoacrylate adhesive. Each sample was fixed to clamps of the test instrument and uniaxially stretched at a constant velocity (10 mm min^{-1}). The applied force-displacement data were recorded during the mechanical tensile test. The shear strength herein was obtained by dividing the failure-state peeling force by the area (length × width) of the elastomer/hydrogel interface.

Functional demonstration of the PEDOT:PSS strain sensor for wearable applications

As shown in Figure 4B, the as-fabricated sensor (elastomer, PDMS; hydrogel, PAAm, first pre-strain, 50%; second pre-strain, 100%) was attached to different parts of the human body for the detection of pulse, phonation, swallowing, facial expressions, and limb movement. The data were recorded using a digital multimeter (Truevolt 34465A, Keysight) and then exported for further analysis. All the demonstrations were performed by the first author with informed consent.

Institutional review board approval for human subject testing

The conducted human subject experiments were performed in compliance with the protocols that have been approved by the institutional review board (IRB) at the University of California, Los Angeles (IRB#17-000170). All subjects gave written informed consent before participation in the study. For all demonstrations on human skin, a signed consent was obtained from the volunteer.

SUPPLEMENTAL INFORMATION

Supplemental information can be found online at https://doi.org/10.1016/j.matt.2021.06.034.

ACKNOWLEDGMENTS

This work was supported by the National Institutes of Health (1R01HL140951-01A1, 1R01HL140618-01), the National Key R&D Program of China (2018YFC1707700) and the start up funds of the University of Hong Kong.

AUTHOR CONTRIBUTIONS

Conceptualization, H. Liu, S.Z., and A.K.; methodology, H. Liu and S.Z.; investigation, H. Liu, Z.L., H. Lin, Y.Z., and S.A.; writing – original draft, H. Liu and S.Z.; writing – review & editing, H. Liu, S.Z., T.J.L., S.E., M.R.D., F.X., and A.K.; funding acquisition, S.Z., F.X., and A.K.; resources, S.Z., F.X., and A.K.; supervision, S.Z., F.X., and A.K.

DECLARATION OF INTERESTS

The authors declare no competing interests.

Received: October 19, 2020
Revised: April 6, 2021
Accepted: June 18, 2021
Published: July 15, 2021

REFERENCES

1. Chung, H.U., Kim, B.H., Lee, J.Y., Lee, J., Xie, Z., Ibler, E.M., Lee, K., Banks, A., Jeong, J.Y., Kim, J., et al. (2019). Binodal, wireless epidermal electronic systems with in-sensor analytics for neonatal intensive care. Science *363*, eaau0780.
2. Yu, X., Xie, Z., Yu, Y., Lee, J., Vazquez-Guardado, A., Luan, H., Ruban, J., Ning, X., Akhtar, A., Li, D., et al. (2019). Skin-integrated wireless haptic interfaces for virtual and augmented reality. Nature *575*, 473–479.
3. Liu, H., Qing, H., Li, Z., Han, Y.L., Lin, M., Yang, H., Li, A., Lu, T.J., Li, F., and Xu, F. (2017). A promising material for human-friendly functional wearable electronics. Mater. Sci. Eng. R *112*, 1–22.
4. Xie, C., Liu, J., Fu, T.-M., Dai, X., Zhou, W., and Lieber, C.M. (2015). Three-dimensional macroporous nanoelectronic networks as minimally invasive brain probes. Nat. Mater. *14*, 1286–1292.
5. Liu, Y., Liu, J., Chen, S., Lei, T., Kim, Y., Niu, S., Wang, H., Wang, X., Foudeh, A.M., Tok, J.B.H., and Bao, Z. (2019). Soft and elastic hydrogel-based microelectronics for localized low-voltage neuromodulation. Nat. Biomed. Eng. *3*, 58–68.
6. Wang, Y., Zhu, C., Pfattner, R., Yan, H., Jin, L., Chen, S., Molina-Lopez, F., Lissel, F., Liu, J., Rabiah, N.I., et al. (2017). A highly stretchable, transparent, and conductive polymer. Sci. Adv. *3*, e1602076.
7. Li, D., Lai, W.-Y., Zhang, Y.-Z., and Huang, W. (2018). Printable transparent conductive films for flexible electronics. Adv. Mater. *30*, 1704738.
8. Oh, J.Y., Kim, S., Baik, H.-K., and Jeong, U. (2016). Conducting polymer dough for deformable electronics. Adv. Mater. *28*, 4455–4461.
9. Li, W., Gao, F., Wang, X., Zhang, N., and Ma, M. (2016). Strong and robust polyaniline-based supramolecular hydrogels for flexible supercapacitors. Angew. Chem. Int. Ed. *55*, 9196–9201.
10. Kim, J., Lee, J., You, J., Park, M.-S., Hossain, M.S.A., Yamauchi, Y., and Kim, J.H. (2016). Conductive polymers for next-generation energy storage systems: recent progress and new functions. Mater. Horiz. *3*, 517–535.
11. Wang, T., Zhang, Y., Liu, Q., Cheng, W., Wang, X., Pan, L., Xu, B., and Xu, H. (2018). A self-healable, highly stretchable, and solution processable conductive polymer composite for ultrasensitive strain and pressure sensing. Adv. Funct. Mater. *28*, 1705551.
12. Zeng, Y., Han, Y., Zhao, Y., Zeng, Y., Yu, M., Liu, Y., Tang, H., Tong, Y., and Lu, X. (2015). Advanced Ti-doped Fe_2O_3@PEDOT core/shell anode for high-energy asymmetric supercapacitors. Adv. Energy Mater. *5*, 1402176.
13. Anothumakkool, B., Soni, R., Bhange, S.N., and Kurungot, S. (2015). Novel scalable synthesis of highly conducting and robust PEDOT paper for a high performance flexible solid supercapacitor. Energy Environ. Sci. *8*, 1339–1347.
14. Cai, G., Darmawan, P., Cui, M., Wang, J., Chen, J., Magdassi, S., and Lee, P.S. (2016). Highly stable transparent conductive silver grid/PEDOT:PSS electrodes for integrated bifunctional flexible electrochromic supercapacitors. Adv. Energy Mater. *6*, 1501882.
15. Zhang, C., Higgins, T.M., Park, S.-H., O'Brien, S.E., Long, D., Coleman, J.N., and Nicolosi, V. (2016). Highly flexible and transparent solid-state supercapacitors based on RuO_2/PEDOT:PSS conductive ultrathin films. Nano Energy *28*, 495–505.
16. Zhang, Y., Cui, W., Zhu, Y., Zu, F., Liao, L., Lee, S.-T., and Sun, B. (2015). High efficiency hybrid PEDOT:PSS/nanostructured silicon Schottky junction solar cells by doping-free rear contact. Energy Environ. Sci. *8*, 297–302.
17. Lee, C.-P., Lai, K.-Y., Lin, C.-A., Li, C.-T., Ho, K.-C., Wu, C.-I., Lau, S.-P., and He, J.-H. (2017). A paper-based electrode using a graphene dot/PEDOT:PSS composite for flexible solar cells. Nano Energy *36*, 260–267.
18. Huang, X., Wang, K., Yi, C., Meng, T., and Gong, X. (2016). Efficient perovskite hybrid solar cells by highly electrical conductive PEDOT:PSS hole transport layer. Adv. Energy Mater. *6*, 1501773.
19. Tan, Z.-K., Moghaddam, R.S., Lai, M.L., Docampo, P., Higler, R., Deschler, F., Price, M., Sadhanala, A., Pazos, L.M., Credgington, D., et al. (2014). Bright light-emitting diodes based on organometal halide perovskite. Nat. Nanotechnol. *9*, 687.
20. Cho, K.-S., Lee, E.K., Joo, W.-J., Jang, E., Kim, T.-H., Lee, S.J., Kwon, S.-J., Han, J.Y., Kim, B.-K., Choi, B.L., and Kim, J.M. (2009). High-performance crosslinked colloidal quantum-dot light-emitting diodes. Nat. Photon. *3*, 341–345.
21. Shi, Z.-F., Sun, X.-G., Wu, D., Xu, T.-T., Zhuang, S.-W., Tian, Y.-T., Li, X.-J., and Du, G.-T. (2016). High-performance planar green light-emitting diodes based on a PEDOT:PSS/$CH_3NH_3PbBr_3$/ZnO sandwich structure. Nanoscale *8*, 10035–10042.
22. Singh, R., Tharion, J., Murugan, S., and Kumar, A. (2017). Ito-free solution-processed flexible electrochromic devices based on PEDOT:PSS as transparent conducting electrode. ACS Appl. Mater. Interfaces *9*, 19427–19435.

23. Malti, A., Gabrielsson, E.O., Crispin, X., and Berggren, M. (2015). An electrochromic bipolar membrane diode. Adv. Mater. *27*, 3909–3914.

24. Ding, Y., Invernale, M.A., and Sotzing, G.A. (2010). Conductivity trends of PEDOT-PSS impregnated fabric and the effect of conductivity on electrochromic textile. ACS Appl. Mater. Interfaces *2*, 1588–1593.

25. Gkoupidenis, P., Schaefer, N., Garlan, B., and Malliaras, G.G. (2015). Neuromorphic functions in PEDOT:PSS organic electrochemical transistors. Adv. Mater. *27*, 7176–7180.

26. Zhang, Y., Inal, S., Hsia, C.-Y., Ferro, M., Ferro, M., Daniel, S., and Owens, R.M. (2016). Supported lipid bilayer assembly on PEDOT:PSS films and transistors. Adv. Funct. Mater. *26*, 7304–7313.

27. Wu, X., Surendran, A., Ko, J., Filonik, O., Herzig, E.M., Müller-Buschbaum, P., and Leong, W.L. (2019). Ionic-liquid doping enables high transconductance, fast response time, and high ion sensitivity in organic electrochemical transistors. Adv. Mater. *31*, 1805544.

28. Zhang, S., Chen, Y., Liu, H., Wang, Z., Ling, H., Wang, C., Ni, J., Saltik, B.C., Wang, X., Meng, X., et al. (2020). Room-temperature-formed PEDOT:PSS hydrogels enable injectable, soft, and healable organic bioelectronics. Adv. Mater. *32*, 1904752.

29. Zhang, S., Ling, H., Chen, Y., Cui, Q., Ni, J., Wang, X., Hartel, M.C., Meng, X., Lee, K., Lee, J., et al. (2020). Hydrogel-enabled transfer-printing of conducting polymer films for soft organic bioelectronics. Adv. Funct. Mater. *30*, 1906016.

30. Wen, Z., Yang, Y., Sun, N., Li, G., Liu, Y., Chen, C., Shi, J., Xie, L., Jiang, H., Bao, D., et al. (2018). A wrinkled PEDOT:PSS film based stretchable and transparent triboelectric nanogenerator for wearable energy harvesters and active motion sensors. Adv. Funct. Mater. *28*, 1803684.

31. Takamatsu, S., Lonjaret, T., Ismailova, E., Masuda, A., Itoh, T., and Malliaras, G.G. (2016). Wearable keyboard using conducting polymer electrodes on textiles. Adv. Mater. *28*, 4485–4488.

32. Trung, T.Q., Ramasundaram, S., Hwang, B.-U., and Lee, N.-E. (2016). An all-elastomeric transparent and stretchable temperature sensor for body-attachable wearable electronics. Adv. Mater. *28*, 502–509.

33. Pang, C., Lee, G.-Y., Kim, T.-i., Kim, S.M., Kim, H.N., Ahn, S.-H., and Suh, K.-Y. (2012). A flexible and highly sensitive strain-gauge sensor using reversible interlocking of nanofibres. Nat. Mater. *11*, 795–801.

34. Gao, Y., Yu, L., Yeo, J.C., and Lim, C.T. (2020). Flexible hybrid sensors for health monitoring: materials and mechanisms to render wearability. Adv. Mater. *32*, 1902133.

35. Ma, Y., Zhang, Y., Cai, S., Han, Z., Liu, X., Wang, F., Cao, Y., Wang, Z., Li, H., Chen, Y., and Feng, X. (2020). Flexible hybrid electronics for digital healthcare. Adv. Mater. *32*, 1902062.

36. Liu, H., Li, M., Ouyang, C., Lu, T.J., Li, F., and Xu, F. (2018). Biofriendly, stretchable, and reusable hydrogel electronics as wearable force sensors. Small *14*, 1801711.

37. Jiang, Y., Liu, Z., Matsuhisa, N., Qi, D., Leow, W.R., Yang, H., Yu, J., Chen, G., Liu, Y., Wan, C., et al. (2018). Auxetic mechanical metamaterials to enhance sensitivity of stretchable strain sensors. Adv. Mater. *30*, 1706589.

38. Wang, C., Li, X., Gao, E., Jian, M., Xia, K., Wang, Q., Xu, Z., Ren, T., and Zhang, Y. (2016). Carbonized silk fabric for ultrastretchable, highly sensitive, and wearable strain sensors. Adv. Mater. *28*, 6640–6648.

39. Roh, E., Hwang, B.U., Kim, D., Kim, B.Y., and Lee, N.E. (2015). Stretchable, transparent, ultrasensitive, and patchable strain sensor for human-machine interfaces comprising a nanohybrid of carbon nanotubes and conductive elastomers. ACS Nano *9*, 6252–6261.

40. Cheng, Y., Wang, R., Sun, J., and Gao, L. (2015). A stretchable and highly sensitive graphene-based fiber for sensing tensile strain, bending, and torsion. Adv. Mater. *27*, 7365–7371.

41. Li, Q., Ullah, Z., Li, W., Guo, Y., Xu, J., Wang, R., Zeng, Q., Chen, M., Liu, C., and Liu, L. (2016). Wide-range strain sensors based on highly transparent and supremely stretchable graphene/Ag-nanowires hybrid structures. Small *12*, 5058–5065.

42. Liu, N., Fang, G., Wan, J., Zhou, H., Long, H., and Zhao, X. (2011). Electrospun PEDOT:PSS–PVA nanofiber based ultrahigh-strain sensors with controllable electrical conductivity. J. Mater. Chem. *21*, 18962.

43. Borghetti, M., Serpelloni, M., Sardini, E., and Pandini, S. (2016). Mechanical behavior of strain sensors based on PEDOT:PSS and silver nanoparticles inks deposited on polymer substrate by inkjet printing. Sens. Actuators A *243*, 71–80.

44. Sun, B., Long, Y.Z., Liu, S.L., Huang, Y.Y., Ma, J., Zhang, H.D., Shen, G., and Xu, S. (2013). Fabrication of curled conducting polymer microfibrous arrays via a novel electrospinning method for stretchable strain sensors. Nanoscale *5*, 7041–7045.

45. Savagatrup, S., Chan, E., Renteria-Garcia, S.M., Printz, A.D., Zaretski, A.V., O'Connor, T.F., Rodriquez, D., Valle, E., and Lipomi, D.J. (2015). Plasticization of PEDOT:PSS by common additives for mechanically robust organic solar cells and wearable sensors. Adv. Funct. Mater. *25*, 427–436.

46. Seyedin, M.Z., Razal, J.M., Innis, P.C., and Wallace, G.G. (2014). Strain-responsive polyurethane/PEDOT:PSS elastomeric composite fibers with high electrical conductivity. Adv. Funct. Mater. *24*, 2957–2966.

47. Ding, Y., Xu, W., Wang, W., Fong, H., and Zhu, Z. (2017). Scalable and facile preparation of highly stretchable electrospun PEDOT:PSS@PU fibrous nonwovens toward wearable conductive textile applications. ACS Appl. Mater. Interfaces *9*, 30014–30023.

48. Klein, M.C., and Gorb, S.N. (2012). Epidermis architecture and material properties of the skin of four snake species. J. R. Soc. Interfaces *9*, 3140–3155.

49. Yang, W., Chen, I.H., Gludovatz, B., Zimmermann, E.A., Ritchie, R.O., and Meyers, M.A. (2013). Natural flexible dermal armor. Adv. Mater. *25*, 31–48.

50. Yang, T., Li, X., Jiang, X., Lin, S., Lao, J., Shi, J., Zhen, Z., Li, Z., and Zhu, H. (2016). Structural engineering of gold thin films with channel cracks for ultrasensitive strain sensing. Mater. Horiz. *3*, 248–255.

51. An, H., Habib, T., Shah, S., Gao, H., Radovic, M., Green, M.J., and Lutkenhaus, J.L. (2018). Surface-agnostic highly stretchable and bendable conductive Mxene multilayers. Sci. Adv. *4*, eaaq0118.

52. Xu, S., Fan, Z., Yang, S., Zhao, Y., and Pan, L. (2021). Flexible, self-powered and multi-functional strain sensors comprising a hybrid of carbon nanocoils and conducting polymers. Chem. Eng. J. *404*, 126064.

53. Fan, X., Wang, N., Yan, F., Wang, J., Song, W., and Ge, Z. (2018). A transfer-printed, stretchable, and reliable strain sensor using PEDOT:PSS/Ag NW hybrid films embedded into elastomers. Adv. Mater. Technol. *3*, 1800030.

54. Peng, S., Wu, S., Yu, Y., Blanloeuil, P., and Wang, C.H. (2020). Nano-toughening of transparent wearable sensors with high sensitivity and a wide linear sensing range. J. Mater. Chem. A *8*, 20531–20542.

55. Li, F., Liu, Y., Shi, X., Li, H., Wang, C., Zhang, Q., Ma, R., and Liang, J. (2020). Printable and stretchable temperature-strain dual-sensing nanocomposite with high sensitivity and perfect stimulus discriminability. Nano Lett. *20*, 6176–6184.

56. Dauzon, E., Lin, Y., Faber, H., Yengel, E., Sallenave, X., Plesse, C., Goubard, F., Amassian, A., and Anthopoulos, T.D. (2020). Stretchable and transparent conductive PEDOT:PSS-based electrodes for organic photovoltaics and strain sensors applications. Adv. Funct. Mater. *30*, 2001251.

57. Jia, Y., Shen, L., Liu, J., Zhou, W., Du, Y., Xu, J., Liu, C., Zhang, G., Zhang, Z., and Jiang, F. (2019). An efficient PEDOT-coated textile for wearable thermoelectric generators and strain sensors. J. Mater. Chem. C *7*, 3496–3502.

58. Li, G., Qiu, Z., Wang, Y., Hong, Y., Wan, Y., Zhang, J., Yang, J., Wu, Z., Hong, W., and Guo, C.F. (2019). PEDOT:PSS/grafted-PDMS electrodes for fully organic and intrinsically stretchable skin-like electronics. ACS Appl. Mater. Interfaces *11*, 10373–10379.

59. Ryu, J., Kim, J., Oh, J., Lim, S., Sim, J.Y., Jeon, J.S., No, K., Park, S., and Hong, S. (2019). Intrinsically stretchable multi-functional fiber with energy harvesting and strain sensing capability. Nano Energy *55*, 348–353.

60. Lee, J.H., Jeong, Y.R., Lee, G., Jin, S.W., Lee, Y.H., Hong, S.Y., Park, H., Kim, J.W., Lee, S.-S., and Ha, J.S. (2018). Highly conductive, stretchable, and transparent PEDOT:PSS electrodes fabricated with triblock copolymer additives and acid treatment. ACS Appl. Mater. Interfaces *10*, 28027–28035.

61. Amjadi, M., Kyung, K.-U., Park, I., and Sitti, M. (2016). Stretchable, skin-mountable, and wearable strain sensors and their potential

applications: a review. Adv. Funct. Mater. *26*, 1678–1698.

62. Liu, H., Li, M., Liu, S., Jia, P., Guo, X., Feng, S., Lu, T.J., Yang, H., Li, F., and Xu, F. (2020). Spatially modulated stiffness on hydrogels for soft and stretchable integrated electronics. Mater. Horiz. *7*, 203–213.

63. Deng, J., Wang, L., Liu, L., and Yang, W. (2009). Developments and new applications of UV-induced surface graft polymerizations. Prog. Polym. Sci. *34*, 156–193.

64. Schneider, M.H., Tran, Y., and Tabeling, P. (2011). Benzophenone absorption and diffusion in poly(dimethylsiloxane) and its role in graft photo-polymerization for surface modification. Langmuir *27*, 1232–1240.

65. Yuk, H., Zhang, T., Parada, G.A., Liu, X., and Zhao, X. (2016). Skin-inspired hydrogel-elastomer hybrids with robust interfaces and functional microstructures. Nat. Commun. *7*, 12028.

66. Duprez, D.A., Kaiser, D.R., Whitwam, W., Finkelstein, S., Belalcazar, A., Patterson, R., Glasser, S., and Cohn, J.N. (2004). Determinants of radial artery pulse wave analysis in asymptomatic individuals. Am. J. Hypertens. *17*, 647–653.